# A Frequency-Modulated Space Vector Pulse-Width Modulation for Ripple Current Control of Permanent-Magnet Motor Drives

Yue Zhao Department of Electrical Engineering University of Arkansas Fayetteville, AR, USA yuezhao@uark.edu

Tyler Adamson Department of Electrical Engineering University of Arkansas Fayetteville, AR, USA tvadamso@email.uark.edu

Juan Carlos Balda Department of Electrical Engineering University of Arkansas Fayetteville, AR, USA jbalda@uark.edu

Yuzhi Zhang US Corporate Research Center ABB Inc. Raleigh, NC, USA yuzhi.zhang@us.abb.com

Abstract—Various methods have been proposed to perform real-time ripple current estimation, which is critical for the performance improvement of ac motor drives. In this work, a novel ripple current prediction (RCP) approach is firstly proposed, which combines the advantages of both equivalent circuit based and machine model based methods. The proposed RCP method is accurate and effective in practical applications. Then a frequency-modulated (FM) space-vector pulse-width modulation (SVPWM) is proposed to actively control the ripple current by adjust the switching frequency on a cycle-bycycle basis. The proposed FM-SVPWM has the capability to maintain the same amount of ripple current using reduced switching frequency or reduce the current ripple without increasing the switching frequency. Extensive simulation studies have been performed to validate the feasibility and effectiveness of the proposed methods.

Keywords—current ripple, permanent-magnet motor drives, pulse-width modulation, variable switching frequency

#### I. INTRODUCTION

Three-phase voltage source inverters (VSI) are widely adopted for the ac motor drive applications, especially in the electric drives for permanent-magnet (PM) motors [1]-[3]. Various modulation techniques [4]-[8], e.g., sinusoidal pulsewidth modulation (PWM), space-vector PWM (SVPWM) discontinuous PWM (DPWM) and etc., can be utilized to translate voltage reference to gates signals, which are further applied to gate drivers to turn the power electronic switches on and off. Due to the switching actions, the motor winding inductances are frequently charged and discharged, which leads to stator current ripples [5]. Analyzing the ripple current introduced by switching actions, which was studied mainly in an offline fashion [9], [10], has led to various enhanced sensing [11], control and modulation approaches [12], [13].

Recently, several real-time ripple current estimation or prediction techniques, using either equivalent circuit (EC) based approach [10], [12] or machine model in rotor (dq)reference frame [13], have been developed. With real-time ripple current information, it is possible to design more accurate dead-time compensation and also variable switching

prediction (RCP) approach, Thevenin equivalent circuits are normally used to model the VSI circuits when certain voltage vectors are applied. The load parameters are indispensable for the EC-RCP approach. Therefore, the EC-RCP approach has good performance for non-salient pole motor drives, e.g., the surface-mounted PM motors, grid-tied inverters, and etc., where load parameters can be accurately measured and are relatively stable during normal operation. For other practical applications, for instance, the ac drives for salient-pole motors, e.g., the interior PM (IPM) motors, the machine model (MM) based RCP has better performance over the EC-RCP. Since MM-RCP is performed in the dq reference frame, which loses the direct link to the switching sequence in each phase. Therefore, the MM-RCP is usually more complicated to implement than the EC-RCP.

In this work, to address the issues with the existing two RCP methods, a novel ripple current prediction scheme is proposed, which combines the advantages of both EC based and MM based RCP methods. The proposed approach is accurate and effective for practical applications. Then a frequency-modulated (FM) SVPWM method is proposed to actively control the ripple current by optimize switching frequency on a cycle-by-cycle basis. The proposed FM-SVPWM has the capability to achieve the same amount of ripple current while using reduced equivalent switching frequency, i.e., the equivalent switching frequency reduction mode, or reduced ripple current amplitude without increasing equivalent switching frequency, i.e., ripple reduction mode. The effectiveness of proposed methods are validated using comprehensive simulation studies.

## II. THE PROPOSED RCP FOR AC DRIVES

As the schematic of a generic two level inverter feeding an IPM motor shown in Fig. 1, node n is the midpoint of the inverter dc link, node N is the neutral point of a three-phase Y-connected IPM motor, while a, b, and c are the inverter output terminals. The switching state of the inverter phase x, i.e.,  $S_x$  (x = a, b, or c), can be either 0 or 1, denoted as  $S_x = [0, 1]$ 1]. When  $S_x = 1$ , the top switch in phase x is on; when  $S_x = 0$ , the bottom switch is on. Then the instantaneous voltage of the inverter output terminal x with respect to node n can be expressed as

$$v_{xn} = \left(2 \cdot S_x - 1\right) \cdot \frac{V_{dc}}{2} \tag{1}$$

while the average of  $v_{xn}$  over one switching period  $(T_s)$  can be expressed as

frequency PWM techniques [12], [13], which may further lead to reduced switching losses, mitigate electromagnetic interference (EMI) and etc. In the EC based ripple current This work was supported in part by the U.S. National Science

Foundation (NSF) under CAREER Award ECCS-1751506 and the NSF Engineering Research Center (ERC) for Power Optimization of Electro-Thermal Systems (POETS) with cooperative agreement EEC-1449548.

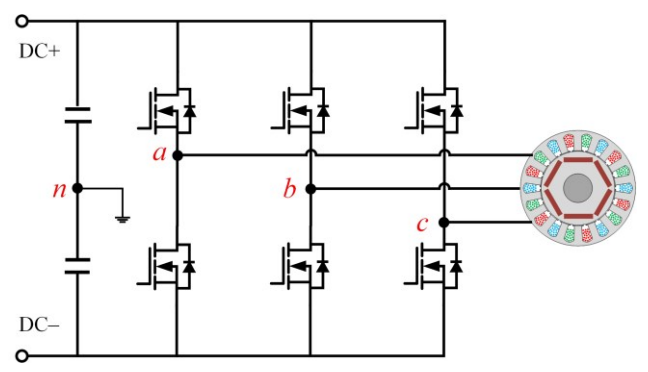


Fig. 1. The schematic of a two-level inverter circuit commonly used in motor drive applications.

$$V_{xn} = (2 \cdot d_x - 1) \cdot \frac{V_{dc}}{2} \tag{2}$$

where  $d_x$  is the duty ratio of the top switch in phase x. The difference between the  $v_{xn}$  and  $V_{xn}$  is the ripple voltage, i.e.,

$$\Delta v_x = v_{xN} - V_{xN} = (S_x - d_x)V_{dc} \tag{3}$$

Applying the Park transformation,  $T_{abc} \rightarrow dq0$ , to the threephase ripple voltage, the resulting ripple voltage in the dqreference frame, i.e.,  $\Delta v_d$  and  $\Delta v_q$ , can be expressed as

$$\begin{cases} \Delta v_d = \frac{2}{3} \left[ \left( \Delta v_b - \Delta v_a \right) \cos \left( \theta - \frac{2\pi}{3} \right) + \left( \Delta v_c - \Delta v_a \right) \cos \left( \theta - \frac{4\pi}{3} \right) \right] \\ \Delta v_q = \frac{2}{3} \left[ \left( \Delta v_a - \Delta v_b \right) \sin \left( \theta - \frac{2\pi}{3} \right) + \left( \Delta v_a - \Delta v_c \right) \sin \left( \theta - \frac{4\pi}{3} \right) \right] \end{cases}$$

$$(4-1 \text{ and } 4-2)$$

where  $\theta$  is the rotor position. Over a short period of time  $\Delta T$ , which is less than a switching cycle, since  $\Delta v_d$  and  $\Delta v_q$  can be viewed as constant, the increment of the ripple currents, i.e.,  $\Delta i_d$  and  $\Delta i_q$ , can be calculated as:

$$\begin{cases} \Delta i_d = \frac{1}{L_d} \int_0^{\Delta T} \Delta v_d \, dt \approx \frac{\Delta v_d \cdot \Delta T}{L_d} \end{cases}$$
 (5-1)

$$\begin{cases} \Delta i_q = \frac{1}{L_a} \int_0^{\Delta T} \Delta v_q \, dt \approx \frac{\Delta v_q \cdot \Delta T}{L_a} \end{cases}$$
 (5-2)

where  $L_d$  and  $L_q$  are the d- and q-axis inductances, respectively. Then applying the inverse Park transformation,  $T_{dq0 \rightarrow abc}$ , to the  $\Delta i_d$  and  $\Delta i_q$  obtained by (5), the increment of ripple current in each phase, i.e.,  $\Delta i_x$ , can be determined. Take phase a as an example,  $\Delta i_a$  can be expressed as a function of  $\Delta T$  as

$$\Delta i_a \left( \Delta T \right) = \Delta i_d \cos \theta - \Delta i_q \sin \theta$$

$$= \frac{L_d + L_q}{3L_d L_q} \cdot \left( \Delta v_a - \frac{1}{2} \Delta v_b - \frac{1}{2} \Delta v_c \right) \cdot \Delta T \qquad (6)$$

$$+ \frac{L_q - L_d}{2L_d L_a} \cdot \Delta v_d'' \cdot \Delta T$$

where 
$$\Delta v_d'' = \frac{2}{3} \begin{bmatrix} (\Delta v_b - \Delta v_a) \cos\left(2\theta - \frac{2\pi}{3}\right) \\ + (\Delta v_c - \Delta v_a) \cos\left(2\theta - \frac{4\pi}{3}\right) \end{bmatrix}$$
, which

shares the same expression as  $\Delta v_d$ , i.e., expression (4-1), but as a function of  $2\theta$ . For non-salient motors and grid-tied applications,  $L_d$  and  $L_q$  are identical, such that the second term in (6) equals to zero and the expression of  $\Delta i_a$  is exactly the same as those derived in [12] using EC based approach. However, since  $L_d$  is not identical to  $L_q$  in the salient-pole motors, the second term in (6) cannot be ignored, otherwise obvious ripple prediction errors can be observed.

Equation (6) is derived in the dq reference frame. Though it improves the accuracy, it lacks the physical meanings compared to analysis performed by directly using three-phase motor line-to-natural voltages and equivalent circuits. When using SVPWM, as shown in Fig. 2, seven switching configurations are applied to the inverter in a predetermined sequence over one  $T_s$ . To capture all possible peaks of ripple current, (6) needs to be calculated seven times during one  $T_s$ , which may be computational intensive for the digital signal processors (DSP).

As shown in Fig. 2, by comparing the  $v_{xn}$  (red solid line) with fundamental voltage (blue dashed line), which is assumed to be constant over one  $T_s$ , the polarity (+ or –) of the ripple current slope can be determined. If  $v_{xn}$  is higher

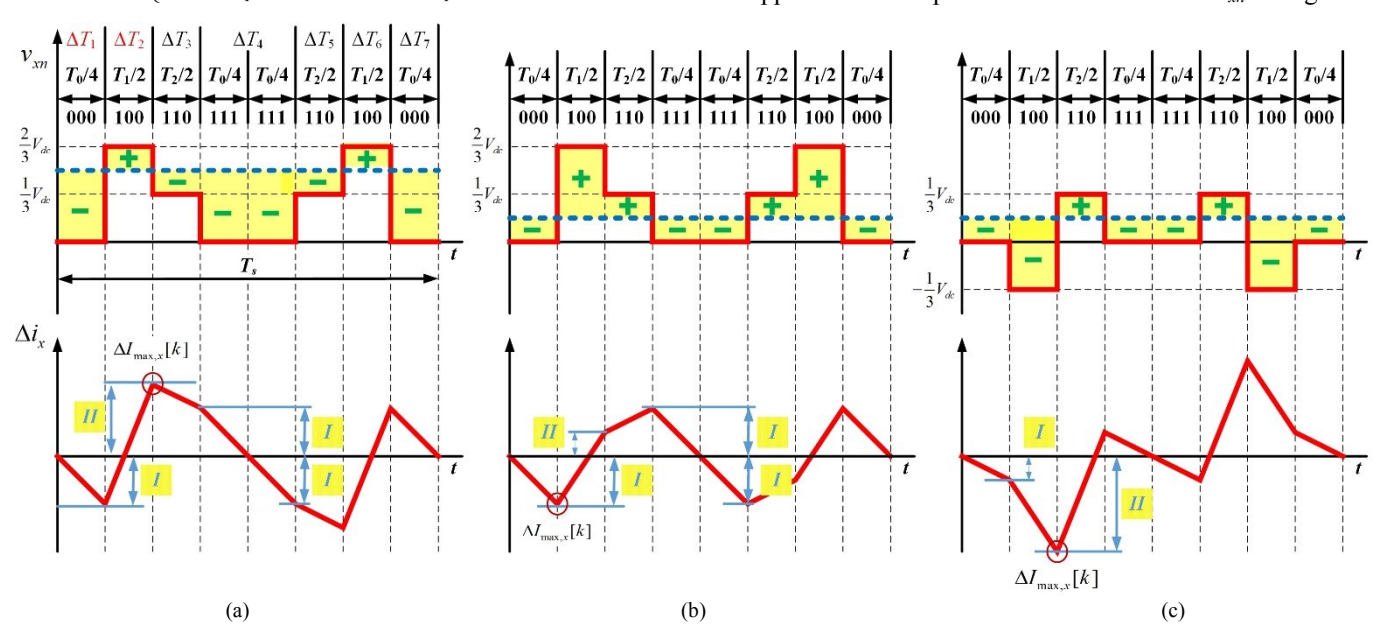


Fig. 2. Three scenarios of ripple current when using SVPWM.

than the fundamental voltage, ripple current slope is positive (+) and ripple current increases. While if  $v_{xn}$  is lower than the fundamental voltage, ripple current slope is negative (-) and ripple current decreases. In addition, over one  $T_s$ , the average value of ripple current is zero. Due to the symmetry of the gate signals generated by SVPWM,  $v_{xn}$  is also symmetric, which further leads to a symmetric ripple current with respect to  $t = T_s/2$ . According to Fig. 2, the predicted peak of the ripple current at the  $k^{th}$  switching cycle, which is denoted as  $\Delta I_{a,max}[k]$ , is the maximum of the I and II, which can be determined as

$$I = \left| \Delta i_a \left( \Delta T \right) \right|_{\Delta T = T_0/4}$$

$$II = \left| \Delta i_a \left( \Delta T \right) \right|_{\Delta T = T_1/2} - I$$
(7)

and

$$\Delta I_{a,\max}[k] = \max(I, II) \tag{8}$$

Therefore, to predict  $\Delta I_{a,max}$ , (6) only needs to be computed twice per switching cycle for all the scenarios when using SVPWM. The flow chart of  $\Delta I_{a,max}$  prediction is showing in Fig. 3. The Table I summarizes the  $\Delta T$  information required by (7).

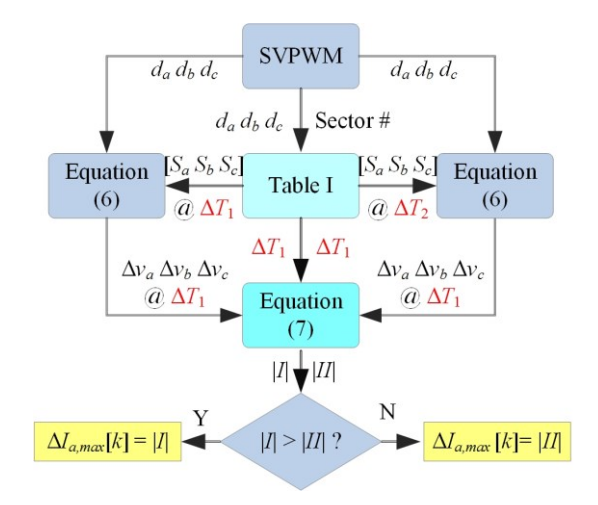


Fig. 3. A flow chart of the proposed  $\Delta I_{a,max}$  prediction.

TABLE I. SWITCHING TIME CALCULATION IN EACH SECTOR.

Sector Number	$\Delta T_1 = T_0/4$	$[S_a S_b S_c]$ during $\Delta T_1$	$\Delta T_2 = T_1/2$	$[S_a S_b S_c]$ during $\Delta T_2$
1	$(1-d_a)\cdot T_s/2$	[0 0 0]	$(d_a-d_b)\cdot T_s/2$	[1 0 0]
2	$(1-d_b)\cdot T_s/2$	$[0\ 0\ 0]$	$(d_b-d_a)\cdot T_s/2$	[0 1 0]
3	$(1-d_b)\cdot T_s/2$	$[0\ 0\ 0]$	$(d_b-d_c)\cdot T_s/2$	[0 1 0]
4	$(1-d_c)\cdot T_s/2$	$[0\ 0\ 0]$	$(d_c-d_b)\cdot T_s/2$	[0 0 1]
5	$(1-d_c)\cdot T_s/2$	$[0\ 0\ 0]$	$(d_c-d_a)\cdot T_s/2$	[0 0 1]
6	$(1-d_a)\cdot T_s/2$	[0 0 0]	$(d_a-d_c)\cdot T_s/2$	[1 0 0]

Simulation results of  $\Delta I_{a,max}$  prediction for an IPM motor are shown in Fig. 4, in which the red circles represent the predicted  $\Delta I_{a,max}$  in every switching cycle, while the blue waveform is the phase a ripple current,  $\Delta i_a$ . For an IPM motor, when compared to the EC based RCP, the accuracy of

can be improved by using the proposed RCP approach. Experimental study is also performed on a 200 W IPM motor drive and the result is shown in Fig. 5, where IPM motor runs at 100 Hz fundamental frequency. The stator current is sensed once per switching cycle at the peak of the carrier signal using DSP. Both current sensed by DSP and current sensed by a high-bandwidth current transducer, which contains the current ripple, are displayed in an oscilloscope. The current ripple is extracted by using the math function in the oscilloscope. As shown in Fig. 5, the predicted  $\Delta I_{a,max}$  well tracked the peak of the actual ripple current.

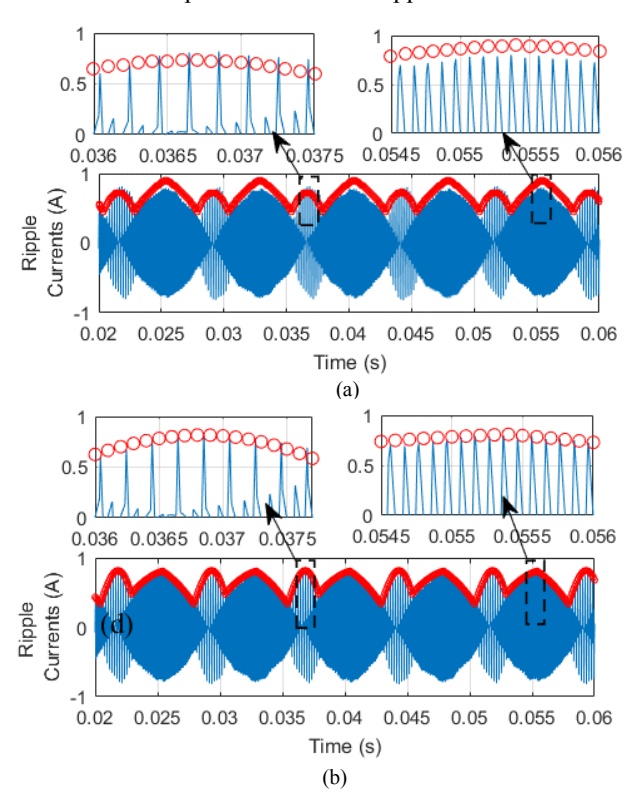


Fig. 4. The performance of ripple current prediction using (a) the equivalent circuits approach and (b) the proposed approach.

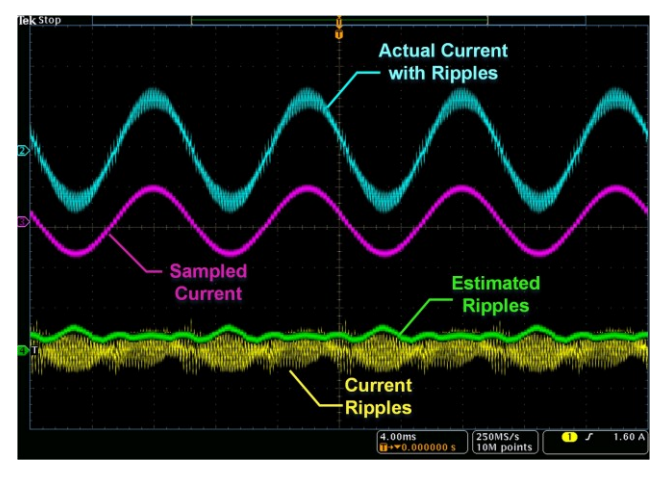


Fig. 5. The performance of the proposed RCP captured by an oscilloscope.

## III. FREQUENCY-MODULATED SVPWM

As shown in Fig. 6, when switching period  $T_s$  is fixed, the peak ripple current is not evenly distributed in the time domain. Over a fundamental electric cycle of an ac motor, i.e.,  $T_f$ , obvious difference exists between the peaks and

valleys of the  $\Delta I_{a,max}$ . According to (6), at  $k^{\text{th}}$  switching cycle, once  $d_x$  is calculated,  $\Delta I_{a,max}$  is determined only by  $\Delta T_1$  (=  $T_0/4$ ) and  $\Delta T_2$  (=  $T_1/2$ ), which all depend on  $T_s$ , e.g., Table I. Considering a balanced 3-phase IPM motor, the maximum among  $\Delta I_{a,max}$ ,  $\Delta I_{b,max}$  and  $\Delta I_{c,max}$  is defined as  $\Delta I_M$ , i.e.,

$$\Delta I_M[k] = \max(\Delta I_{a,\max}[k], \Delta I_{b,\max}[k], \Delta I_{c,\max}[k])$$
 (9)

It is possible to reshape the profile of  $\Delta I_M$  by properly adjusting  $T_s$  on a cycle-by-cycle basis.

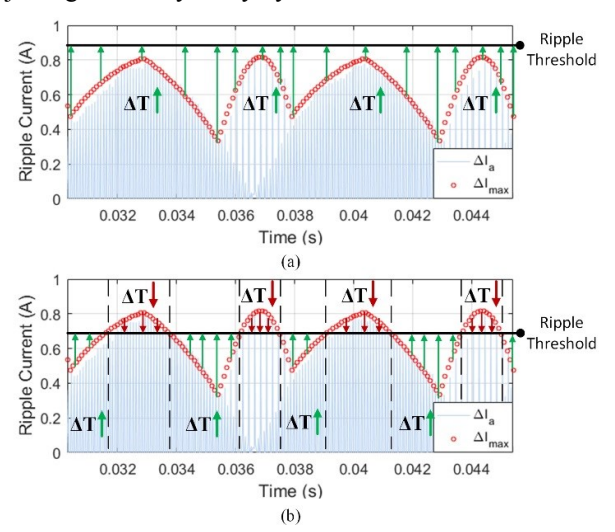


Fig. 6. Two operating modes of the proposed FM-SVPWM (a) equivalent switching frequency reduction mode and (b) ripple current reduction mode.

#### A. The Proposed FM-SVPWM

In this work,  $f_n$  is defined as the nominal switching frequency, which is the switching frequency that can be used by the constant switching frequency SVPWM to meet the predetermined allowable peak ripple current, i.e.,  $\Delta I_M^*$ .  $T_n = 1/f_n$  is defined as the nominal switching cycle.

During the  $k^{th}$  switching cycle, the sector number of the voltage vector and  $d_x$  to be applied for the  $(k+1)^{th}$  switching cycle are determined by SVPWM algorithm. Still in the  $k^{th}$  switching cycle, using the  $T_n$  information, the  $\Delta I_M[k+1]$  can be predicted using the algorithm illustrated in Fig. 3. This predicted  $\Delta I_M[k+1]$  stands for the peak ripple current in the  $(k+1)^{th}$  switching cycle, if the switching period for the next switching cycle is  $T_n$ .

To actively control the  $\Delta I_M$ , in this work, the actual switching cycle used for modulation, i.e.,  $T_{sw} = 1/f_{sw}$ , is optimized throughout a fundamental electric cycle by using

$$T_{sw} = \left(1 + \gamma \frac{\eta \cdot \Delta I_{M}^{*} - \Delta I_{M}}{\Delta I_{M}}\right) T_{n}$$
 (9)

where  $\gamma$  is a parameter to determine the slope of the  $f_{sw}$  with respect to the ratio of  $\Delta I_M/\Delta I^*_M$ ;  $\eta$  is a parameter to determine the operating mode of the FM-SVPWM.

As shown in Fig. 6(a), when  $\eta$  is greater than 1, which means ripple threshold is even larger than the predetermined  $\Delta I_M^*$  at nominal switching frequency, then obviously the period of each switching cycle can be increased, while maintaining the ripple current within the threshold. Since  $T_{sw}$  are increased, the equivalent switching frequency ( $f_{eq}$ ), which is defined as the total number of the switching cycles divided by  $T_f$ , is reduced, so as the switching losses.

As shown in Fig. 6(b), if  $\eta$  is smaller than 1, which means ripple threshold is less than  $\Delta I_M^*$ ,  $T_{sw}$  is optimized to reduce the peak of ripple current. In this operating mode, over one  $T_f$ , the  $f_{sw}$  is reduced during some switching cycles, while increased in others. Therefore, the average switching frequency over one  $T_f$  depends on the value of  $\eta$ . If  $\eta$  is close to 1, both switching loss reduction and ripple reduction can be achieved simultaneously. If  $\eta$  is much smaller than 1, the aggressive ripple reduction can be achieved at the cost of increased switching losses.

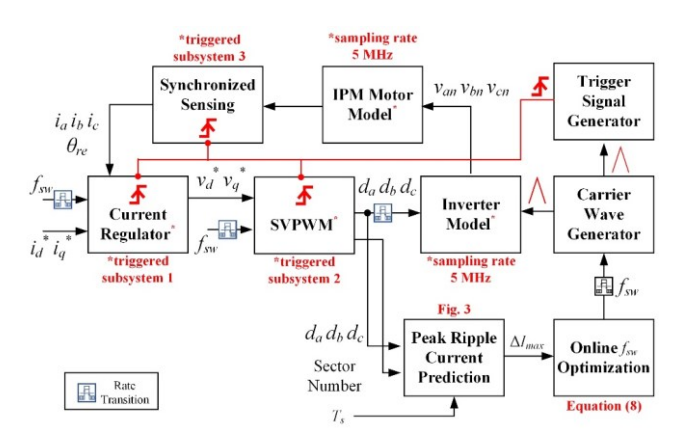


Fig. 7. An overall block diagram of the discrete-time simulation model.

### B. The Model used in Simulation Studies

To validate the feasibility and effectiveness of the proposed FM-SVPWM, a comprehensive simulation study is performed in Matlab Simulink. The overall block diagram of the designed discrete-time multi-rate simulation model is illustrated in Fig. 7.

In the model of the field oriented controller (FOC), the discrete-time proportional-integral (PI) controller with feedforward compensation is adopted in the current regulator, which generates the voltage references  $v_d^*$  and  $v_q^*$ . The standard SVPWM is utilized in this model. However, the  $T_{sw}$ can be updated in each switching cycle. During the  $k^{th}$ switching cycle, using the three-phase duty ratio and sector number obtained from the SVPWM for the  $(k+1)^{th}$  switching cycle,  $\Delta I_M$  [k+1] can be determined by the peak ripple current predictor, which is designed based on Fig. 3. The predicted  $\Delta I_M$  [k+1], is a critical input of the online  $f_{sw}$ optimization block, which is executed once per switching cycle to determine the optimal  $f_{sw}$  for the  $(k+1)^{th}$  switching cycle. The optimal  $f_{sw}$  is not only used by the carrier wave generator, which generates the triangular carrier waveform for each switching cycle, but also the discrete-time integration in the PI current regulator and SVPWM block. Both the current regulator and SVPWM are all implemented as triggered subsystems. Based on the carrier waveform, one trigger signal is generated per switching cycle, such that current regulator and SVPWM are also executed once per switching cycle.

Both inverter model and IPM motor model run at 5 MHz sampling frequency. The current sensing scheme, which is synchronized to the peak of the carrier waveform, is also implemented in the simulation. The major specifications of the IPM motor used in this simulation study are listed in Table II. The nominal switching frequency is 10 kHz.

TABLE II. SPECIFICATIONS OF THE IPM MOTOR USED IN THE SIMULATION STUDIES

Specifications	IPM Motor	
Nominal Speed	3,000 rpm	
Rated Power	200 W	
EMF Constant	0.0138 V·s/rad	
Stator Resistance	$0.235~\Omega$	
$L_d$	0.275 mH	
$L_q$	0.364 mH	
# of Pole Pairs	4	
$f_s$	10 kHz	

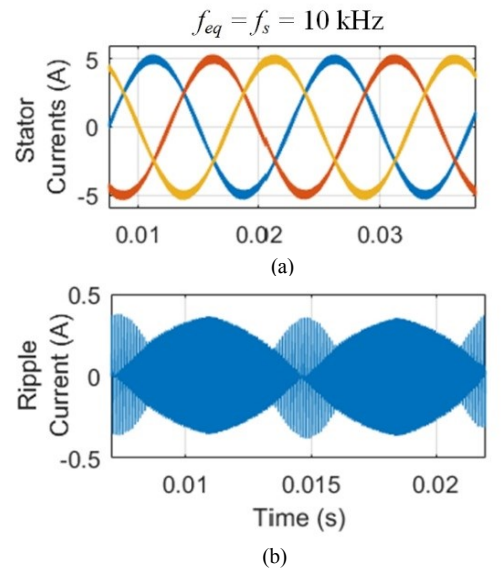


Fig. 8. Simulation results at 1,000 rpm using constant 10 kHz switching frequency: (a) three phase stator currents and (b) phase *a* ripple current.

# C. Simulation Results for Mode $1 - f_{eq}$ Reduction

Several cases are studied using the designed simulation model to validate the effectiveness of the FM-SVPWM in  $f_{eq}$  reduction mode. In the first case, the IPM motor runs at 1,000 rpm with the nominal switching frequency at 10 kHz and ripple threshold at 0.5 A. When using constant 10 kHz

switching frequency, the maximum ripple current is around 0.4 A. The motor is controlled using constant switching frequency at the very beginning, while the FM-SVPWM is enabled at t = 0.05s. When constant switching frequency is used, the results, including three phase current and phase a ripple current, are shown in Fig. 8. Once FM-SVPWM is enabled and operated in the  $f_{eq}$  reduction mode, i.e.,  $\eta > 1$ , as shown in Fig. 9, the instantaneous switching frequency immediately start to deviate from 10 kHz and update on a cycle-by-cycle basis. By selecting different  $\eta$ , the  $f_{eq}$  can be reduced without increasing the maximum of the ripple current, e.g., Fig. 9(a) and (b). The zoomed in figures for the instantaneous switching frequency and stator currents are shown in Fig. 10, when  $f_{eq} = 9.05$  kHz. When further increasing  $\eta$  to reduce  $f_{eq}$  to 8.53 kHz, which is 15% switching frequency reduction, the maximum ripple current is increased compared to that using the nominal switching frequency. However, the peak ripple current is still within 0.5 A, as shown in Fig. 9(c).

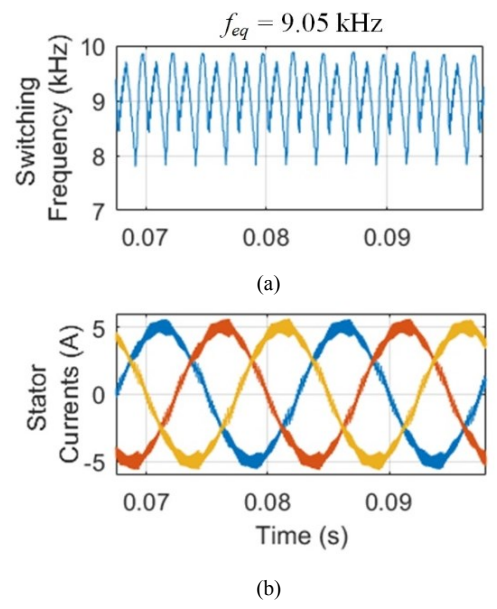


Fig. 10. Simulation results at 1,000 rpm using FM-SVPWM with  $f_{eq} = 9.05$  kHz: (a) instantaneous switching frequency and (b) three phase stator currents.

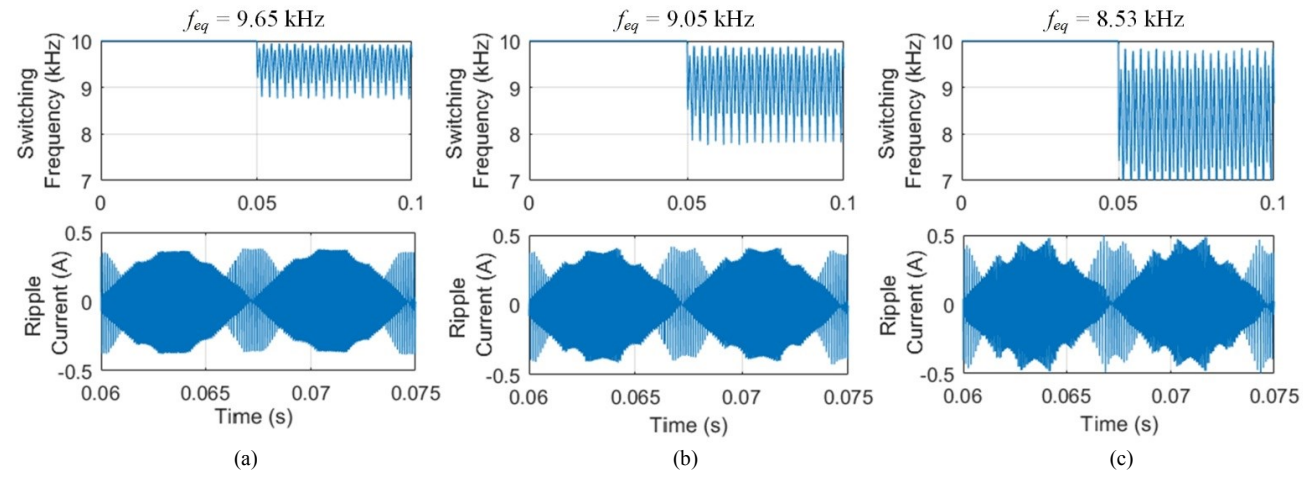


Fig. 9. Simulation results at 1,000 rpm using FM-SVPWM: (a)  $f_{eq} = 9.65$  kHz, (b)  $f_{eq} = 9.05$  kHz, and (c)  $f_{eq} = 8.53$  kHz. In each subfigure, the top is the instantons switching frequency and the bottom is the details of the current ripple from 0.06s to 0.075s.

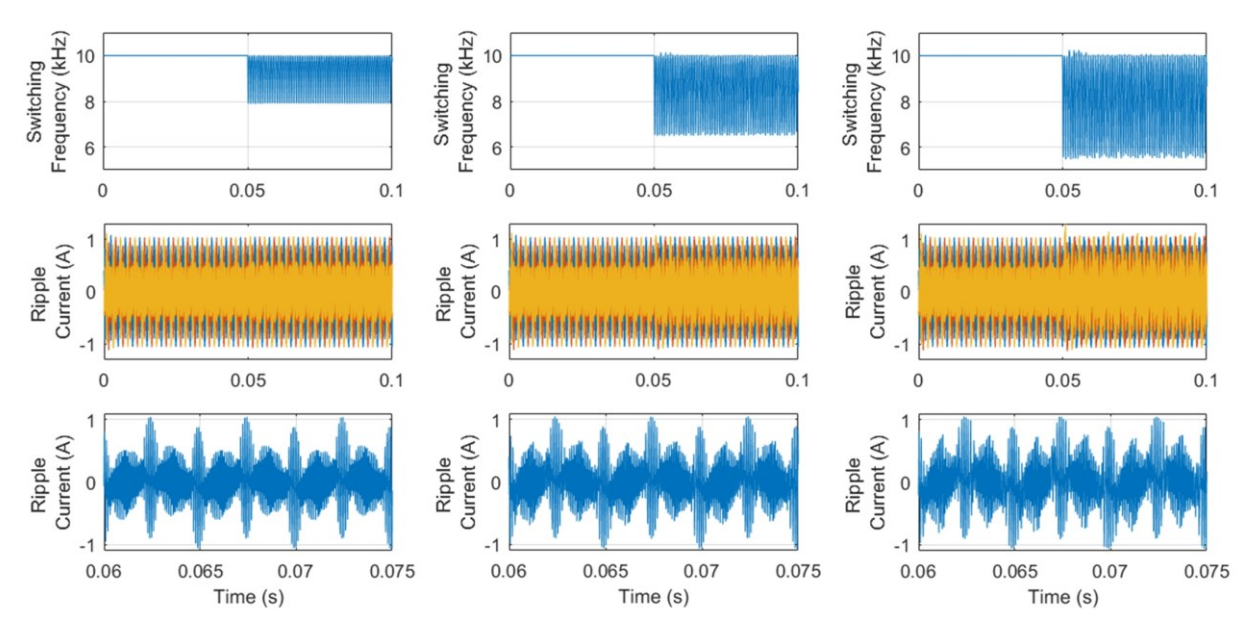


Fig. 11. Simulation results at 3,000 rpm using FM-SVPWM: (a)  $f_{eq} = 9.15$  kHz, (b)  $f_{eq} = 8.35$  kHz, and (c)  $f_{eq} = 7.92$  kHz. In each subfigure, the top is the instantons switching frequency, the middle is the ripple current and the bottom is the zoomed in current ripple from 0.06s to 0.075s.

In the second case, the IPM motor runs at it's nominal speed 3,000 rpm with the nominal switching frequency at 10 kHz and ripple threshold at 1.0 A. The FM-SVPWM is also enabled at t = 0.05s. As shown in Fig. 11, by using the proposed scheme, up to 20%  $f_{eq}$  reduction can be achieved without violating the 1.0 A threshold for the peak current ripple. The comparison of the stator currents between constant 10 kHz switching frequency modulation and FM-SVPWM with  $f_{eq} = 9.15$  kHz is shown in Fig. 12.

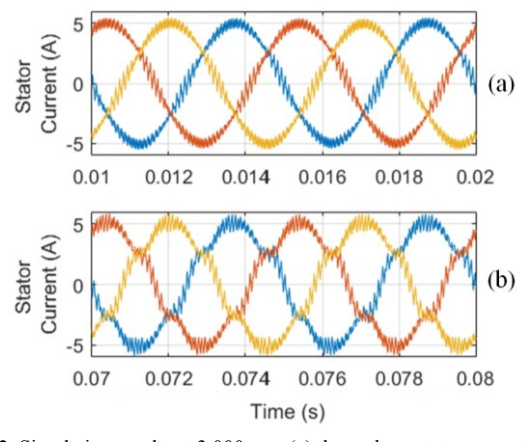


Fig. 12. Simulation results at 3,000 rpm (a) three phase stator currents when using constant 10 kHz switching frequency and (b) three phase stator currents when using FM-SVPWM with  $f_{eq} = 9.15$  kHz.

#### D. Simulation Results for Mode $2 - \Delta I_{\rm M}$ Reduction

To validate the effectiveness of the FM-SVPWM in  $\Delta I_M$  reduction mode, various  $\eta$ , which are all great than 1, have been evaluated in the simulation model. When the IPM motor runs at 1,000 rpm with 10 kHz nominal switching frequency, the maximum the ripple current is 0.38 A. In the  $\Delta I_M$  reduction mode,  $\Delta I_M^*$  is set to be 0.35 A. As shown in Fig. 13, when the proposed scheme is enabled at t=0.05s, the instantaneous switching frequency starts to oscillate around 10 kHz and the  $\Delta I_M$  starts to drop. Especially, as

shown in Fig. 14(a), the zoomed in ripple current waveform clearly shows that its maximum value decreased under 0.35 A, after the FM-SVPWM works in the  $\Delta I_M$  reduction mode. In the meantime, the  $f_{eq}$  is still less than 10 kHz.

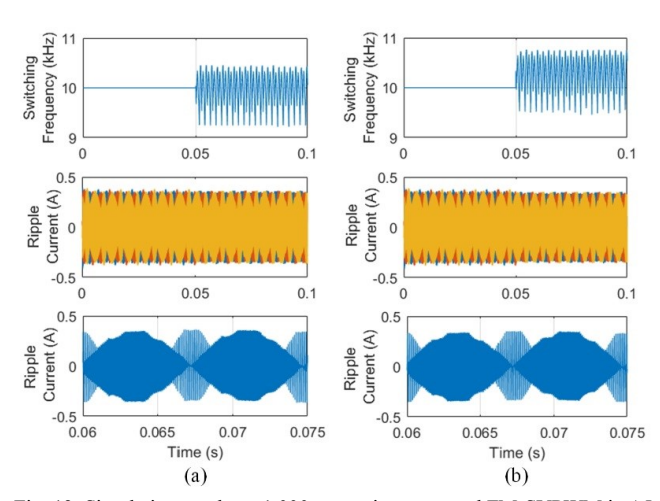


Fig. 13. Simulation results at 1,000 rpm using proposed FM-SVPWM in  $\Delta I_M$  reduction mode: (a)  $f_{eq} = 9.53$  kHz and (b)  $f_{eq} = 9.95$  kHz.

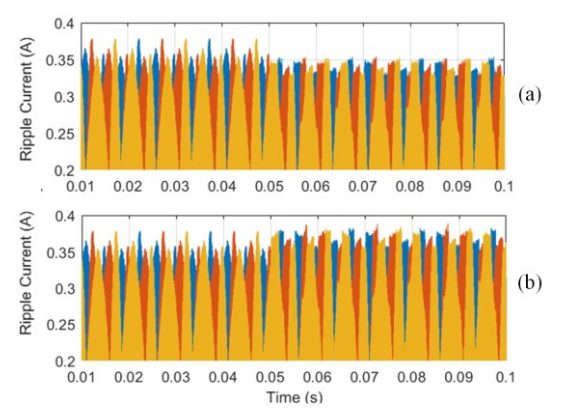


Fig. 14. Simulation results of ripple current at 1,000 rpm when FM-SVPWM is enabled at 0.05 (a) in  $\Delta I_M$  reduction mode and (b) in  $f_{eq}$  reduction mode.

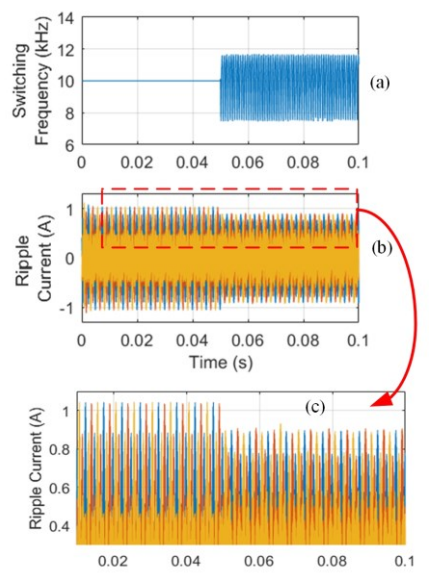


Fig. 15. Simulation results of FM-SVPWM in  $\Delta I_M$  reduction mode at 3,000 rpm (a) instantaneous switching frequency, (b) ripple current and (c) zoomed in ripple current.

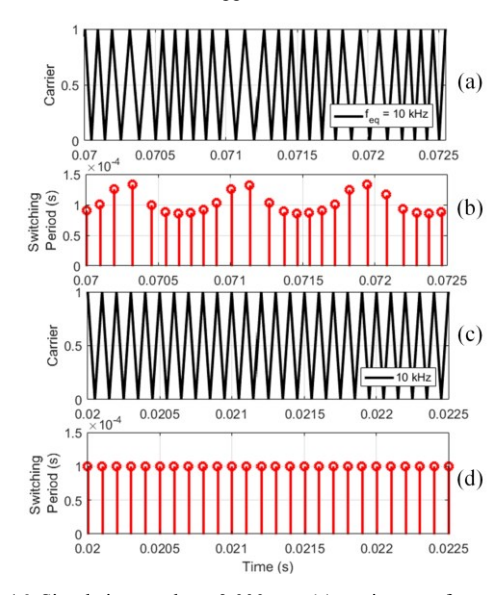


Fig. 16. Simulation results at 3,000 rpm (a) carrier waveform and (b) switching period when using FM-SVPWM, (c) carrier waveform and (d) switching period when using constant frequency SVPWM.

The performance of the proposed FM-SVPWM in  $\Delta I_M$  reduction mode when the IPM motor runs at 3,000 rpm is shown in Fig. 15. Using constant 10 kHz switching frequency, the maximum current ripple is around 1.0 A. After the  $\Delta I_M$  reduction mode enabled at 0.05s, as shown in Fig. 15(c), maximum current ripple drops 0.9 A, which means over 10% ripple reduction can be achieved in this case. The comparison of carrier waveform and switching period between the FM-SVPWM and constant frequency SVPWM are shown in Fig. 16.

### IV. CONCLUSIONS

In this paper, an accurate and effective ripple current prediction approach is proposed for ac motor drives. Based on the real-time predicted peak ripple current, a novel FM-SVPWM is proposed to actively control the ripple current. The proposed FM-SVPWM has two operating modes, i.e., equivalent switching frequency reduction and maximum ripple current reduction. The operating mode can be easily selected by choosing proper parameter  $\eta$ . Comprehensive simulation studies have been performed to validate the feasibility and effectiveness of the proposed RCP approach and FM-SVPWM.

#### REFERENCES

- T. M. Jahns, G. B. Kliman and T. W. Neumann, "Interior Permanent-Magnet Synchronous Motors for Adjustable-Speed Drives," in *IEEE Transactions on Industry Applications*, vol. IA-22, no. 4, pp. 738-747, July 1986.
- [2] K. T. Chau, C. C. Chan and C. Liu, "Overview of Permanent-Magnet Brushless Drives for Electric and Hybrid Electric Vehicles," in *IEEE Transactions on Industrial Electronics*, vol. 55, no. 6, pp. 2246-2257, June 2008.
- [3] Y. Zhao, W. Qiao and L. Wu, "An Adaptive Quasi-Sliding-Mode Rotor Position Observer-Based Sensorless Control for Interior Permanent Magnet Synchronous Machines," in *IEEE Transactions on Power Electronics*, vol. 28, no. 12, pp. 5618-5629, Dec. 2013.
- [4] M. P. Kazmierkowski and L. Malesani, "Current control techniques for three-phase voltage-source PWM converters: a survey," in IEEE Transactions on Industrial Electronics, vol. 45, no. 5, pp. 691-703, Oct 1998.
- [5] D. G. Holmes, and T. A. Lipo, Pulse Width Modulation for Power Converters: Principles and Practice, 1<sup>st</sup> edition, Wiley-IEEE Press, 10/2/2003.
- [6] A. M. Hava, R. J. Kerkman and T. A. Lipo, "Simple analytical and graphical methods for carrier-based PWM-VSI drives," in *IEEE Transactions on Power Electronics*, vol. 14, no. 1, pp. 49-61, Jan 1000
- [7] J. Holtz, "Pulsewidth modulation for electronic power conversion," in Proceedings of the IEEE, vol. 82, no. 8, pp. 1194-1214, Aug 1994.
- [8] J. Rodriguez et al., "Predictive Current Control of a Voltage Source Inverter," in *IEEE Transactions on Industrial Electronics*, vol. 54, no. 1, pp. 495-503, Feb. 2007.
- [9] H. van der Broeck and H. Skudelny, "Analytical analysis of the harmonic effects of a PWM AC drive," *IEEE Trans. Power Electron.*, vol. 3, no. 2, pp. 216-223, Apr 1988.
- [10] G. Grandi, J. Loncarski and O. Dordevic, "Analysis and Comparison of Peak-to-Peak Current Ripple in Two-Level and Multilevel PWM Inverters," *IEEE Trans. Industrial Electron.*, vol. 62, no. 5, pp. 2721-2730, May 2015.
- [11] L. Jarzebowicz, "Errors of a Linear Current Approximation in High-Speed PMSM Drives," in *IEEE Transactions on Power Electronics*, vol. 32, no. 11, pp. 8254-8257, Nov. 2017.
- [12] D. Jiang and F. Wang, "Variable Switching Frequency PWM for Three-Phase Converters Based on Current Ripple Prediction," *IEEE Trans. Power Electron.*, vol. 28, no. 11, pp. 4951-4961, Nov. 2013.
- [13] F. Yang, A. R. Taylor, H. Bai, B. Cheng and A. Khan, "Using d-q transformation to vary switching frequency for interior permanent magnet synchronous motor drive systems," in *IEEE Trans. Transportation Electrification*, vol. 1, no. 3, pp. 277-286, Oct. 2015.